Arabian Journal for Science and Engineering (2023) 48:3209–3225
https://doi.org/10.1007/s13369-022-07114-8

RESEARCH ARTICLE-MECHANICAL ENGINEERING

Predictive Modeling of Surface Roughness and Feed Force in Al-50wt% Si Alloy Milling Based on Response Surface Method and Various Optimal Algorithms

Lu Jing[1] · Qiulin Niu[1] · Dilei Zhan[1] · Shujian Li[1] · Wenhui Yue[1]

Received: 21 March 2022 / Accepted: 28 June 2022 / Published online: 1 August 2022

Abstract
Al-50wt% Si alloy is considered as a difficult-to-machine material and is lack of precision machining research. In this paper, the response surface methodology (RSM), artificial neural network (ANN) and genetic algorithm (GA) are coupled to determine the optimum cutting conditions leading to the minimum surface roughness R_a and feed force F_t in Al-50wt% Si alloy precision milling. The purpose is to address the problem of machining parameters optimization in precision milling high Si-Al alloy. The R_a and F_t were considered as two process responses and cutting speed (v_c), feed per tooth (f_z), radial cutting depth (a_e) and axial cutting depth (a_p) were the process parameters. Using the rotatable orthogonal central composite design, 31 experiments were conducted. Based on RSM and analysis of variance (ANOVA), the influence of milling parameters on R_a and F_t was studied. The ANN was also employed for developing R_a and F_t predictive models, and its predictive capability was more accurate compared with RSM. Parameter optimizations were performed for minimizing R_a and F_t in single-objective and multi-objective cases using GA. In multi-objective optimization, the entropy weight method (EWM) was also implemented. Finally, the optimal parameter combination for precision milling Al-50wt% Si alloy was obtained as $v_c = 105$ m/min, $f_z = 0.013$ mm/z, $a_e = 3.909$ mm and $a_p = 0.14$ mm. The prediction errors were found as 3.27% and 4.65% for R_a and F_t, respectively. The results showed the effectiveness of the predictive model and the optimization method.

Keywords Al-50wt% Si alloy · Response surface methodology · Artificial neural network · Genetic algorithm · Multi-objective optimization

1 Introduction

With the increase in requirements in aerospace, automotive, electronic packaging and other fields for material properties, particle reinforced metal matrix composites (PMMC) have attracted more and more attention [1]. This is due to their excellent and attractive comprehensive properties, such as high specific strength and specific stiffness, corrosion resistance, wear resistance, low density and good dimensional stability [2, 3].

Silicon aluminum (Si-Al) alloy is a kind of PMMC. From the microstructure of Si-Al alloy, the reinforced Si particles are dispersed in the soft pure Al matrix [4]. Al-50wt% Si alloy is a typical difficult-to-machine material due to its high Si weight fraction of up to 50%. The machinability of high Si-Al alloy (Si content $\geq$ 30wt%) is much worse than that of other aluminum alloys [5]. It is easy to produce both sticky chips and scratches on the processed workpiece [6]. During machining, plastic deformation occurs in the Al matrix, while elastic deformation, brittle failure or falling off occur in the Si particles [7]. The two-phase material with opposite properties directly leads to the formation of microcracks, pits, edge breakage and other defects on the machined surface [8, 9]. These defects destroy the Si-Al alloy surface accuracy and increase the surface roughness (R_a), which limit its application in industrial production [10].

R_a is an important factor in controlling machining performance [11]. If the R_a of parts is not ideal, it will accelerate the wear of the mating surface, increase the corrosion and reduce the fatigue strength of parts [12]. Thus, optimization techniques must be applied for reducing R_a. Surface roughness is influenced by various factors, including cutting

✉ Qiulin Niu
qlniu2009@163.com

[1] School of Mechanical Engineering, Hunan University of Science and Technology, Xiangtan 411201, People's Republic of China

parameters, cutting environments, tool variables, workpiece variables, etc. [13, 14]. For a specific manufacturing process, it is very challenging to consider all the factors affecting R_a. Among them, the proper setting of cutting parameters is the most crucial [15].

Recently, various process parameter optimization methods and prediction models have been developed. For example, using response surface methodology (RSM) and artificial neural network (ANN), Kumar and Chauhan [16] revealed that the feed rate is determined as the most influential parameter on R_a in turning MMC. Chandrasekaran and Devarasiddappa [17] conducted end milling SiC_p/Al studies using fuzzy logic. They believed that R_a value has a linear relationship with the feed rate and an inverse relationship with the spindle speed. Meanwhile, the increase of SiC particles directly led to linear increase of R_a. Research [18] also showed that the larger the volume and size of reinforcement, the higher the R_a and burr height in machining.

In other researches, Pare et al. [19] used Al_2O_3 + SiC MMC as work material and applied gravitational search algorithms (GSA) to optimize milling parameters. The results showed that GSA has better prediction effect on R_a than genetic algorithm (GA). Zhu et al. [20] established the theoretical model of R_a for Al alloy and SiC based on the expectation theory. Through the exponential composition function, the R_a prediction model of SiC_p/Al MMC was obtained. Finally, the rapid non-dominated sequencing genetic algorithm (NSGA-II) was utilized to optimize grinding parameters.

During machining, various multi-objective optimization problems have also been successfully solved [21–23]. Tamang and Chandrasekaran [24] used RSM and ANN to establish R_a and tool wear VB prediction models for turning SiC_p/Al. The GA and desirability function analysis (DFA) were employed for developing the optimal parameter combination of multi-objective optimization. The minimum values of R_a and VB reached 3.24 μm and 0.327 mm, respectively. Muguthu et al. [25] used feed rate, cutting speed, cutting depth and tools as input parameters in turning SiC_p/Al composites. Tool wear, R_a and specific power consumption were output responses. The results indicated that for R_a, the significant factor is tool insert, followed by cutting speed. For the specific power consumption, the crucial factor is tool insert, followed by feed rate.

The change trends of cutting force influence heat generation, surface accuracy, machine vibration and power consumption, which play a significant role in the cutting process [26, 27]. Therefore, Daniel et al. [28] took the cutting force and surface roughness as multi-objective optimization indices. It was concluded that the R_a decreases with increase in cutting speed and TiB_2 ratio in AA7075/TiB_2 composites machining. The increase in feed and cutting depth caused an increase in cutting force. From the ANOVA, the highest contributor to both indicators was the TiB_2 reinforcement. Karabulut [29] performed milling AA7039/Al_2O_3 tests based on the Taguchi design and ANN. It was found that the material structure is the most important factor affecting R_a and feed rate is the dominant factor affecting cutting force. Tsao and Hocheng [30] carried out an experiment in drilling composites. Through multi-variable regression analysis and radial basis function network (RBFN), the correlations of feed rate, spindle speed and drill diameter with thrust force and R_a were obtained. Utilizing RSM, Premnath et al. [31] optimized cutting force and surface roughness in milling AA6061/Al_2O_3. They observed that the feed rate and Al_2O_3 weight fraction are the two dominant factors affecting the above indicators.

From the literature review, most research mainly focuses on the optimization of cutting parameters in SiC_p/Al composites and other metal alloy matrix composites, few studies have focused on Si-Al alloys, especially Si-Al alloys with high weight fraction. Furthermore, there is also a lack of research on the precision machining of high Si-Al alloy.

To fill the research gap, the multi-objective optimization of four milling parameters (i.e., cutting speed, feed per tooth, radial cutting depth and axial cutting depth) was carried out in this paper to minimize the surface roughness and cutting force during Al-50wt% Si alloy precision milling. Firstly, the significance of regression models and cutting parameters is analyzed by ANOVA, and the influence of cutting parameters on response values is explored. Secondly, predictive modeling was developed and compared by RSM and ANN techniques. Finally, the GA and entropy weight method (EWM) were implemented to optimize machining parameters in single-objective and multi-objective cases. The flowchart for experimentation and analysis is schematically represented in Fig. 1.

This paper solves the problem of machining parameters optimization in precision milling high Si-Al alloy and forms the effective prediction method based on various algorithms. It provides a useful reference for the selection of high Si-Al alloy milling parameters.

2 Experimental

2.1 Workpiece and equipment setup

The workpiece used was the Al-50wt% Si alloy block with a shape of 30 × 25 × 20 mm, and its mechanical properties is listed in Table 1. Figure 2 shows the microstructure of Al-50wt% Si alloy prepared by spray deposition technique. Spray deposition is a material preparation method in which molten metal is centrifugally atomized, then the atomized liquid particles are sprayed on a rotating deposition carrier to form the deposition billet, and the billet is directly rolled

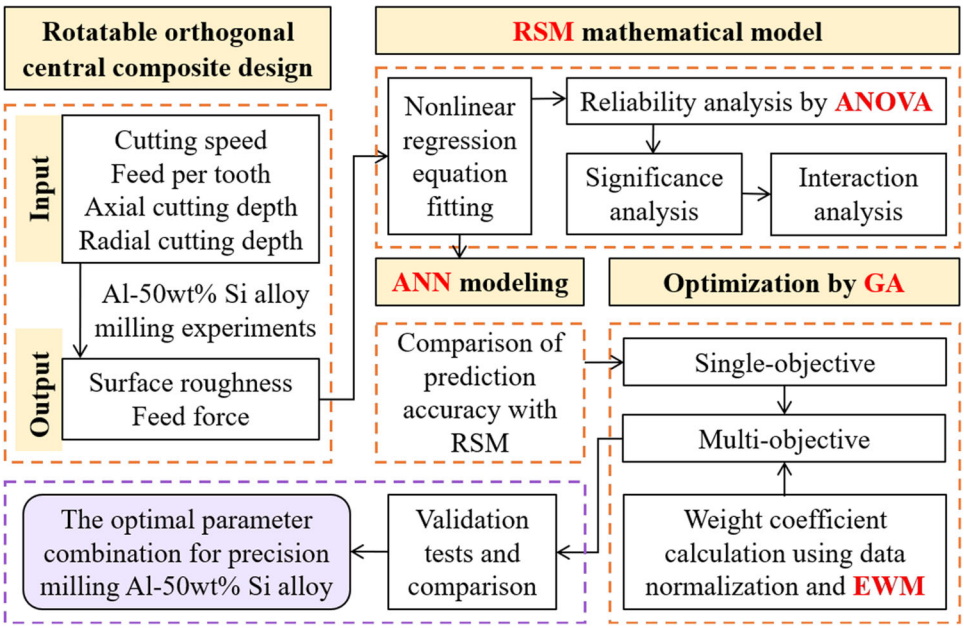

Fig. 1 Block diagram showing the procedure for experimentation and analysis

Table 1 Mechanical properties of Al-50wt% Si alloy

Density (g/cm^3)	Yield strength (MPa)	Coefficient of thermal expansion (ppm/°C)	Thermal conductivity (W/mK) at 25 °C	Strength of extension (MPa)	Young's modulus (GPa)
2.5	210	11.5	140	220	108

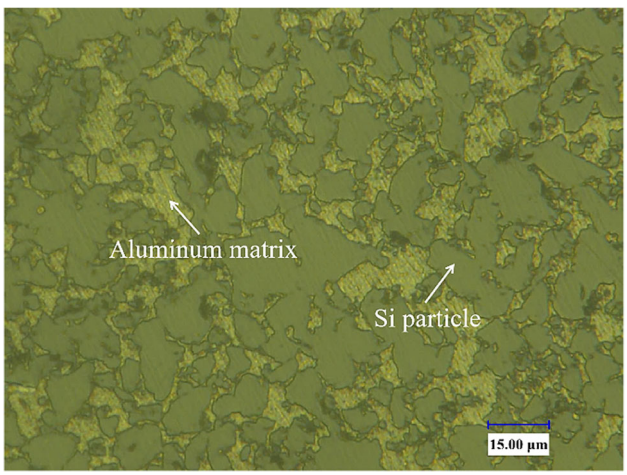

Fig. 2 Microstructure of Al-50wt% Si alloy

[32]. It can be observed from Fig. 2 that the polyhedral Si particles with many sharp corners are surrounded by pure aluminum matrix, and the average size of Si particles is about 10 μm.

Four-edged cemented carbide end milling tools with a diameter of 6 mm (JHP780060E2R030.0Z4-M64) were utilized. The tool tip zone was covered with TiAlN coating. The tool nose radius was 0.3 mm, the rake angle was 10°, the clearance angle was 12°, and the helix angle was 44°.

The experiments of milling Al-50wt% Si alloy were conducted on the KVC800/1 vertical machining center. Figure 3 shows the experimental system. After experimentation, the surface roughness was measured by the instrument JITAI820. Repeat the measurement of workpiece surface roughness under each group of cutting parameters for 6 times, and then take the average value. The cutting force was acted on the three-way piezoelectric sensor Kistler 9253B23. The scanning electron microscope was applied to observe the machined surface morphology, whose type was SU3500.

2.2 Experimental Design

The rotatable orthogonal central composite design was used to conduct Al-50wt% Si alloy milling experiments. This method can ensure that the design provides equal accuracy estimation in all directions, which depicted in Fig. 4. In this paper, the number of factor points (estimate the linear and interactive terms) is 16; the number of axial points (estimate the quadratic term) is 8. The repetitions of the center point to ensure uniformity and precision are 7. They make up 31 sets of experiments.

The four cutting parameters of the (A_v) cutting speed, (B_f) feed per tooth, (C_e) radial cutting depth and (D_p) axial cutting

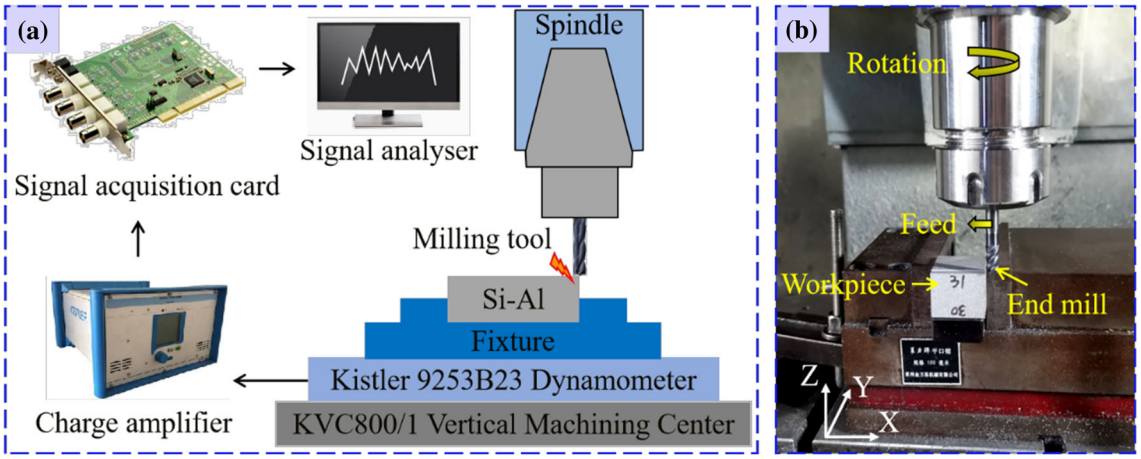

Fig. 3 Schematic illustration of the Al-50wt% Si alloy milling experimental setup: **a** schematic diagram, **b** experimental site map

Table 2 Process parameters with their values at five levels

Control parameters	Code symbol	Unit	Levels				
			−2	−1	0	1	2
Cutting speed, v_c	A_v	m/min	25	45	65	85	105
Feed per tooth, f_z	B_f	mm/z	0.01	0.02	0.03	0.04	0.05
Radial cutting depth, a_e	C_e	mm	2	3	4	5	6
Axial cutting depth, a_p	D_p	mm	0.1	0.2	0.3	0.4	0.5

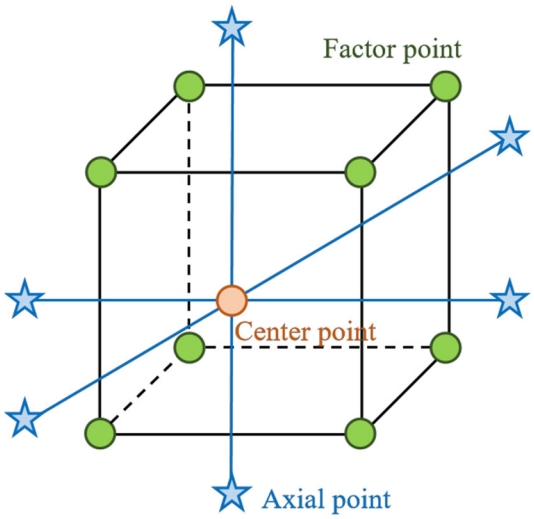

Fig. 4 Rotatable center composite design

depth were the input factors. According to the milling experience and the recommendation given by the tool manufacturer, the factor levels were selected in the range of obtaining precision surface quality of Al-50wt% Si alloy [33]. The process parameters and their values at five levels are given in Table 2. The experimental data of 31 groups are shown in Table 3.

2.3 Experimental Results

Due to the addition of reinforced Si particles, the removal behavior of Si-Al alloy is different from that of ordinary elastic–plastic materials. During processing, brittle Si particles are wrapped by plastic aluminum matrix, and they produce dislocation movement together. Figure 5a illustrates the formation mechanism of Si-Al alloy machined surface caused by particle removal. It can be seen that the cutting process is accompanied by particle breakage, shearing, spalling, cracking, pressing, etc. The Al-50wt% Si alloy machined surface morphology is shown in Fig. 5b. There are large holes, pits, microcracks, Al matrix covering, matrix tearing and other defects on the machined surface.

These machining defects directly impact the surface roughness profile of Si-Al alloy. As exhibited in Fig. 5c, the surface roughness profile curve mainly consists of mixed fracture of Si particles and Al matrix, as well as pits or bulges caused by Si particles. For some specific high Si-Al alloy parts in aerospace, the surface roughness is required to be very high, which reaches 0.4 μm. This paper is intended to solve this problem.

Figure 5d depicts the milling force with time. The milling force mainly includes radial force (F_x), feed force (F_y) and axial force (F_z). The mechanical energy consumed by feed force is the largest due to the large load on the tool in the

Table 3 Cutting parameters and experimental data

Run	Coded factors				Actual factors				Response variable	
	A_v	B_f	C_e	D_p	v_c	f_z	a_e	a_p	R_a (μm)	F_t (N)
1	−1	−1	−1	−1	45	0.02	3	0.2	0.318	25.81
2	1	−1	−1	−1	85	0.02	3	0.2	0.341	23.12
3	−1	1	−1	−1	45	0.04	3	0.2	0.362	26.32
4	1	1	−1	−1	85	0.04	3	0.2	0.540	24.17
5	−1	−1	1	−1	45	0.02	5	0.2	0.396	26.87
6	1	−1	1	−1	85	0.02	5	0.2	0.401	23.64
7	−1	1	1	−1	45	0.04	5	0.2	0.501	28.16
8	1	1	1	−1	85	0.04	5	0.2	0.550	24.06
9	−1	−1	−1	1	45	0.02	3	0.4	0.301	26.63
10	1	−1	−1	1	85	0.02	3	0.4	0.314	28.12
11	−1	1	−1	1	45	0.04	3	0.4	0.387	31.99
12	1	1	−1	1	85	0.04	3	0.4	0.476	31.06
13	−1	−1	1	1	45	0.02	5	0.4	0.410	23.01
14	1	−1	1	1	85	0.02	5	0.4	0.448	26.63
15	−1	1	1	1	45	0.04	5	0.4	0.448	32.38
16	1	1	1	1	85	0.04	5	0.4	0.582	31.84
17	−2	0	0	0	25	0.03	4	0.3	0.314	19.07
18	2	0	0	0	105	0.03	4	0.3	0.424	23.86
19	0	−2	0	0	65	0.01	4	0.3	0.279	22.40
20	0	2	0	0	65	0.05	4	0.3	0.614	33.94
21	0	0	−2	0	65	0.03	2	0.3	0.320	28.94
22	0	0	2	0	65	0.03	6	0.3	0.519	27.49
23	0	0	0	−2	65	0.03	4	0.1	0.428	25.63
24	0	0	0	2	65	0.03	4	0.5	0.597	34.11
25	0	0	0	0	65	0.03	4	0.3	0.403	27.62
26	0	0	0	0	65	0.03	4	0.3	0.478	26.67
27	0	0	0	0	65	0.03	4	0.3	0.406	29.00
28	0	0	0	0	65	0.03	4	0.3	0.417	26.12
29	0	0	0	0	65	0.03	4	0.3	0.382	27.45
30	0	0	0	0	65	0.03	4	0.3	0.397	28.75
31	0	0	0	0	65	0.03	4	0.3	0.433	27.30

feed direction. The special structure of Si-Al alloy makes the milling force unstable, which is easy to cause edge collapse or brittle fracture. Smaller cutting force is helpful to improve the material surface quality and reduce the subsurface damage [34]. Therefore, the main cutting force F_y and surface roughness R_a are selected as the response values in this paper.

3 Response Surface Methodology Model

Response surface methodology (RSM) is a method that combines the principles of mathematics and statistics. RSM uses empirical formula model to approximate the relationship between an output parameter and several input parameters, reconstruct the characteristic function [35]. Furthermore, interactions, the relationship between prediction and actual results, and the 3D response surfaces corresponding to each analysis of variance are constructed.

In this work, RSM is used to study the mathematical relationship between the responses (R_a and F_t) and the independent variables (v_c, f_z, a_e, a_p) in milling Al-50wt% Si alloy. For a response surface model, the quantitative form of relationship between response variables and independent variables can be represented as:

$$y = f(x_1, x_2, x_3 \ldots x_n) + \varepsilon \quad (1)$$

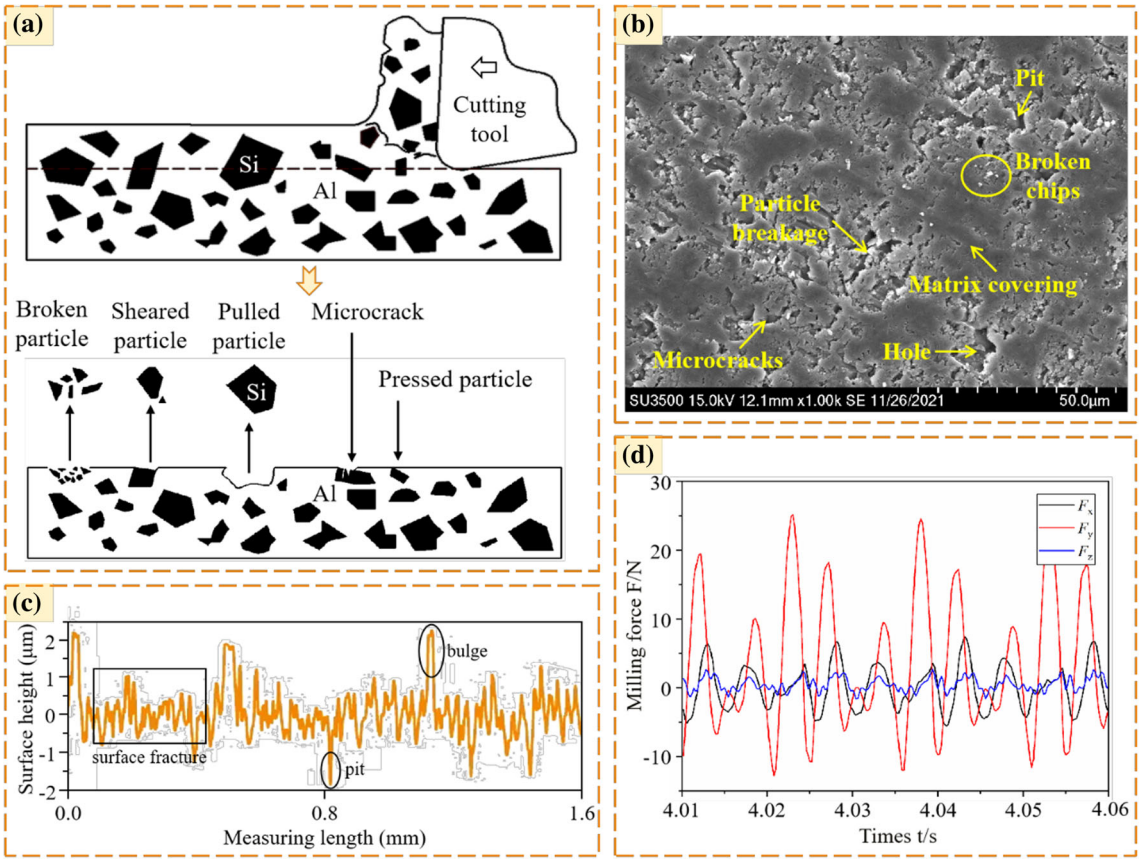

Fig. 5 **a** Schematic diagram of Si-Al alloy machined surface formation caused by particle removal, **b** Al-50wt% Si alloy machined surface morphology, **c** surface roughness profile curve, **d** milling force with time

where y is the output variable, x_1, x_2, x_3 … x_n are input variables, and ε is the error term.

Considering the linear effects, interaction effects and quadratic effects between input factors, quadratic mathematical regression is usually used to establish the relationship between the output response and input parameters. It is expressed as:

$$y = \beta_0 + \sum_{i=1}^{k} \beta_i x_i + \sum_{i=1}^{k} \sum_{j=1, i<j}^{k} \beta_{ij} x_i x_j + \sum_{i=1}^{k} \beta_{ii} x_i^2 + \varepsilon \quad (2)$$

where β_0 is a constant or free term, β_i, β_{ii} and β_{ij} reveal the coefficients of linear, quadratic and interaction term, respectively.

3.1 Regression Equation

Using Design-Expert software, the regression models for R_a and F_t in Al-50wt% Si alloy milling were obtained. Four different types of RSM mathematical models, namely linear, linear with interaction, linear with square and quadratic equations for prediction of surface roughness y_{R_a}, are as follows:

(a) Linear model:

$$y_{R_a} = -0.093822 + 0.00156 v_c + 6.6125 f_z + 0.045625 a_e + 0.122917 a_p \quad (3)$$

(b) Linear with interaction model:

$$y_{R_a} = 0.081459 - 0.001133 v_c + 2.14531 f_z + 0.050391 a_e - 0.078802 a_p + 0.115938 v_c f_z - 0.000241 v_c a_e + 0.000594 v_c a_p - 0.40625 f_z a_e - 4.8125 f_z a_p + 0.076875 a_e a_p \quad (4)$$

(c) Linear with square model:

$$y_{R_a} = -0.033133 + 0.006153 v_c + 3.46696 f_z + 0.057685 a_e - 1.18164 a_p - 0.000035 v_c^2 + 52.4256 f_z^2 - 0.001507 a_e^2 + 2.17426 a_p^2 \quad (5)$$

(d) Quadratic model:

$$y_{R_a} = 0.142149 + 0.00346 v_c - 1.00022 f_z + 0.06245 a_e - 1.38336 a_p - 0.000035 v_c^2$$

$$+ 52.4256 f_z^2 - 0.001507 a_e^2 + 2.17426 a_p^2 + 0.115938 v_c f_z - 0.000241 v_c a_e + 0.000594 v_c a_p - 0.40625 f_z a_e - 4.8125 f_z a_p + 0.076875 a_e a_p \quad (6)$$

When four types of mathematical models are used to fit F_t, it is found that only the pure error term fitted by quadratic model is not significant. In other words, linear, linear with interaction and linear with square equations are not suitable for the fitting of F_t. Therefore, here only lists the quadratic equation for prediction of feed force y_{F_t}:

$$y_{F_t} = 26.37705 + 0.403558 v_c - 292.97991 f_z - 1.55645 a_e - 67.89799 a_p - 0.003732 v_c^2 + 1833.77976 f_z^2 + 0.194628 a_e^2 + 60.8378 a_p^2 - 2.15937 v_c f_z + 0.000094 v_c a_e + 0.494063 v_c a_p + 40.1875 f_z a_e + 1225.625 f_z a_p - 4.53125 a_e a_p \quad (7)$$

3.2 Reliability Analysis of the Model

All regression models were analyzed by analysis of variance (ANOVA) and suitability test to judge their significance. F value is the ratio of regression mean square to residual mean square. P value is the probability under the corresponding F value, indicating the significance of the model. The significance level α takes 0.05 as the criterion of significance and 0.001 as the criterion of extremely significance. It can be seen from Table 4 that the values of P are less than 0.001 for all R_a and F_t regression models, indicating that these models are very significant.

The fitting degree of the models can be verified by adjusted coefficient of determination (Adj R^2) and correlation coefficient (R^2). Among them, R^2 will increase with the increase in independent variables number, while the influence of independent variables number is considered in Adj R^2. Therefore, the optimal regression equation refers to the one with the largest Adj R^2. According to this, the quadratic models are found better in predicting the R_a and F_t in Al-50wt% Si alloy milling. Quadratic models are selected among all models; their equations are shown in Eqs. 6 and 7.

3.3 Significance Analysis of Regression Coefficient

To obtain the most significant cutting parameters that affect the R_a and F_t, Table 5 presents a significant analysis on the regression coefficient.

In the significance analysis for R_a, it can be seen the P value < 0.0001, which means that the probability of excessive noise of the model is only 0.5%. This model is extremely significant. The P value of the mismatch term is 0.1878, which greater than 0.05. Therefore, the lack of fit term is not significant. The regression equation is well fitted. It is also known from Table 5 that the P values of f_z, a_e and v_c are both < 0.05, indicating that they have significant individual effects on R_a. The most influential cutting parameter on R_a is the feed rate f_z. The increase of f_z will significantly increase the defects such as pits, microcracks and aluminum matrix tearing on the Si-Al alloy machined surface due to the pulling out and crushing of Si particles. Therefore, R_a value is increased with the increase of f_z. The response value of R_a also contains the significant interaction term $v_c f_z$ and the significant quadratic term ${a_p}^2$.

As in the above analysis, f_z, a_p, $f_z a_p$, $v_c a_p$, ${v_c}^2$ are significant model terms in the response value of F_t. Feed rate f_z is the most significant cutting parameter on F_t. The increase of f_z leads to the increment of Si-Al alloy cutting thickness and milling force.

Significance analysis of regression coefficient about surface roughness R_a:

(1) Individual effect: $f_z > a_e > v_c > a_p$;
(2) Interaction effect: $v_c f_z > a_e a_p > f_z a_p > v_c a_e > f_z a_e > v_c a_p$;
(3) Quadratic effect: ${a_p}^2 > {v_c}^2 > {f_z}^2 > {a_e}^2$.

Significance analysis of regression coefficient about feed force F_t:

(1) Individual effect: $f_z > a_p > a_e > v_c$;
(2) Interaction effect: $f_z a_p > v_c a_p > a_e a_p > v_c f_z > f_z a_e > v_c a_e$;
(3) Quadratic effect: ${v_c}^2 > {a_p}^2 > {a_e}^2 > {f_z}^2$.

3.4 Response Surface Plots and Contour Maps

Figure 6 indicates the pairwise interactive influence between v_c, f_z, a_e and a_p on R_a, which are sorted according to the influence degree. In each figure, the other two default milling parameters take the 0 level in Table 2.

As shown in Fig. 6a, when the v_c is constant, the R_a increases with the increase of f_z. However, the influence of v_c on R_a is not uniform when the f_z is fixed. This is due to the fact that when the v_c and f_z are small, the cutting force and heat generated are small. The holding force of Al matrix on Si particles reduces the probability of Si particles being pulled out. When the v_c is high, the main removal form of Si particles changes to shear removal, which effectively reduces the defects such as pits or holes. Therefore, when f_z is small and v_c is the lowest (25 m/min) or highest (105 m/min), the minimum R_a can be obtained. However, the influence of v_c is strengthened with the increase of f_z. When the f_z and v_c are both higher, Si particles are easy to be pulled out and pressed

Table 4 Test of significance of RSM models

Run	RSM model	*P* value		*F* value		R^2 (%)		Adj R^2 (%)	
		R_a	F_t	R_a	F_t	R_a	F_t	R_a	F_t
1	Linear	< 0.0001	–	19.87	–	75.35	–	71.56	–
2	Linear with interaction	< 0.0001	–	7.87	–	79.73	–	69.59	–
3	Linear with square	< 0.0001	–	15.01	–	84.52	–	78.89	–
4	Quadratic	< 0.0001	< 0.0001	9.15	9.55	88.90	89.31	79.19	79.96

Table 5 Significance analysis of regression coefficient

Source	Sum of squares	DOF	Mean square	*F* value	*P* value	Remarks
Surface roughness						
Model	0.2146	14	0.0153	9.14	< 0.0001	Significant
v_c	0.0234	1	0.0234	13.93	0.0018	
f_z	0.1049	1	0.1049	62.56	< 0.0001	
a_e	0.0500	1	0.0500	29.78	< 0.0001	
a_p	0.0036	1	0.0036	2.16	0.1609	
v_c^2	0.0057	1	0.0057	3.39	0.0843	
f_z^2	0.0008	1	0.0008	0.4749	0.5006	
a_e^2	0.0001	1	0.0001	0.0369	0.8500	
a_p^2	0.0136	1	0.0136	8.09	0.0117	
$v_c f_z$	0.0086	1	0.0086	5.13	0.0378	
$v_c a_e$	0.0004	1	0.0004	0.2209	0.6447	
$v_c a_p$	0.0000	1	0.0000	0.0135	0.9091	
$f_z a_e$	0.0003	1	0.0003	0.1574	0.6968	
$f_z a_p$	0.0004	1	0.0004	0.2209	0.6447	
$a_e a_p$	0.0009	1	0.0009	0.5637	0.4637	
Residual	0.0268	16	0.0017			
Lack of fit	0.0209	10	0.0021	2.1	0.1878	Not significant
Pure error	0.0060	6	0.0010			
Col Total	0.2415	30				
Feed force						
Model	324.82	14	23.20	9.55	< 0.0001	Significant
v_c	0.0459	1	0.0459	0.0189	0.8924	
f_z	100.98	1	100.98	41.56	< 0.0001	
a_e	0.5192	1	0.5192	0.2137	0.6501	
a_p	89.98	1	89.98	37.03	< 0.0001	
v_c^2	63.73	1	63.73	26.23	0.0001	
f_z^2	0.9616	1	0.9616	0.3957	0.5382	
a_e^2	1.08	1	1.08	0.4458	0.5139	
a_p^2	10.58	1	10.58	4.36	0.0532	
$v_c f_z$	2.98	1	2.98	1.23	0.2842	
$v_c a_e$	0.0001	1	0.0001	0.0000	0.9962	
$v_c a_p$	15.62	1	15.62	6.43	0.0220	
$f_z a_e$	2.58	1	2.58	1.06	0.3178	
$f_z a_p$	24.03	1	24.03	9.89	0.0063	

Table 5 (continued)

Source	Sum of squares	DOF	Mean square	*F* value	*P* value	Remarks
$a_e a_p$	3.29	1	3.29	1.35	0.2620	
Residual	38.88	16	2.43			
Lack of fit	32.44	10	3.24	3.02	0.0943	Not significant
Pure error	6.44	6	1.07			
Col total	363.70	30				

in, worsen the R_a. This is due to the dual action of f_z and v_c, which increases the heat in the cutting zone and softens the Al matrix.

It is worth mentioning that with the increase of a_p, the R_a of the workpiece decreases first and then increases, which can be observed in Fig. 6c, e, f. This is because the actual main deflection angle increases with the increase of a_p [36]. It effectively buffers the instantaneous impact force of tool cutting into Si-Al alloy, and makes the cutting heat distribution more uniform. When the a_p exceeds the tool nose radius (0.3 mm), the spiral tool cutting edge also participates in milling. Increased forces and vibrations result in a decline in machining accuracy.

In Fig. 6, the small graphs with the contour line density basically unchanged show that the interaction between the paired factors and R_a is not significant.

Figure 7 shows the two groups of interactions that have the greatest effect on F_t. From Fig. 7a, it can be seen that increasing both f_z and a_p can increase the F_t. The increased cutting force will aggravate the crack propagation between Si particles and Al substrate. The periodic crack damage on the machined surface reduces the workpiece surface integrity. Therefore, Fig. 7a is consistent with Fig. 6d. Figure 7b shows that lower or higher v_c combined with lower a_p results in lower F_t.

4 Artificial Neural Network Modeling

In the previous part, the quantitative laws between the response values (R_a and F_t) and the input factors (v_c, f_z, a_e, a_p) were obtained by RSM, and the input parameters that affect the response values and the interactions among them were evaluated. However, the established quadratic regression equations based on RSM do not consider the high-order interaction between the impact factors, which may lead to the decline of model accuracy. Fortunately, artificial neural network (ANN) can make up for the shortage of RSM. ANN has the characteristics of high adaptability and strong fitting ability. The three-layer back propagation neural network can fit any function with a certain precision.

ANN is a mathematical or computational model that imitates the structure and function of biological neural network. Neural network is composed of many neurons. There is no connection between the neurons in the same layer, but the adjacent layers are connected by full interconnection. Each neuron input has multiple connection channels, and each connection channel corresponds to a connection weight coefficient [37]. ANN can summarize quantitative laws from complex data. However, so far there are few clear rules that can serve as a basis for obtaining the precision machined surface of Al-50wt% Si alloy. The output of neuron is abstracted into a specific mathematical model as:

$$T = f(P \times \omega + b) \tag{8}$$

where P is the input signal of neuron, ω is the associated weight and is responsible for network adjustment, b is the threshold value of triggering neuron activity, and f is the transfer function.

Back propagation (BP) neural network algorithm takes the square of network error as the objective function and uses the gradient descent method to calculate the minimum value of the objective function [38]. A standard BP network consists of input layer, hidden layer and output layer. In Al-50wt% Si alloy milling, it is applied to predict surface roughness and feed force (R_a, F_t) as functions of four input parameters namely, cutting speed, feed per tooth, radial cutting depth and axial cutting depth (v_c, f_z, a_e, a_p). The BP neural network architecture is shown in Fig. 8. The network is modeled in MATLAB. In this paper, the number of hidden layer neurons is set to 10. *Tansig* is the transfer function of hidden layer neurons, *purelin* is the linear transfer function of output layer neurons, and *trainlm* is the default training function.

From the 31 datasets obtained from milling Si-Al alloy experiments, 21 datasets are selected to train the ANN model, and 10 datasets are used to test the ANN model. In the aspect of network training, the performance of ANN model is evaluated by the mean squared error (MSE) between the predicted and experimental outputs of R_a and F_t. Aiming for MSE with 0.001, successful training can be achieved. The R^2 values of R_a and F_t models during training are 0.969 and 0.980,

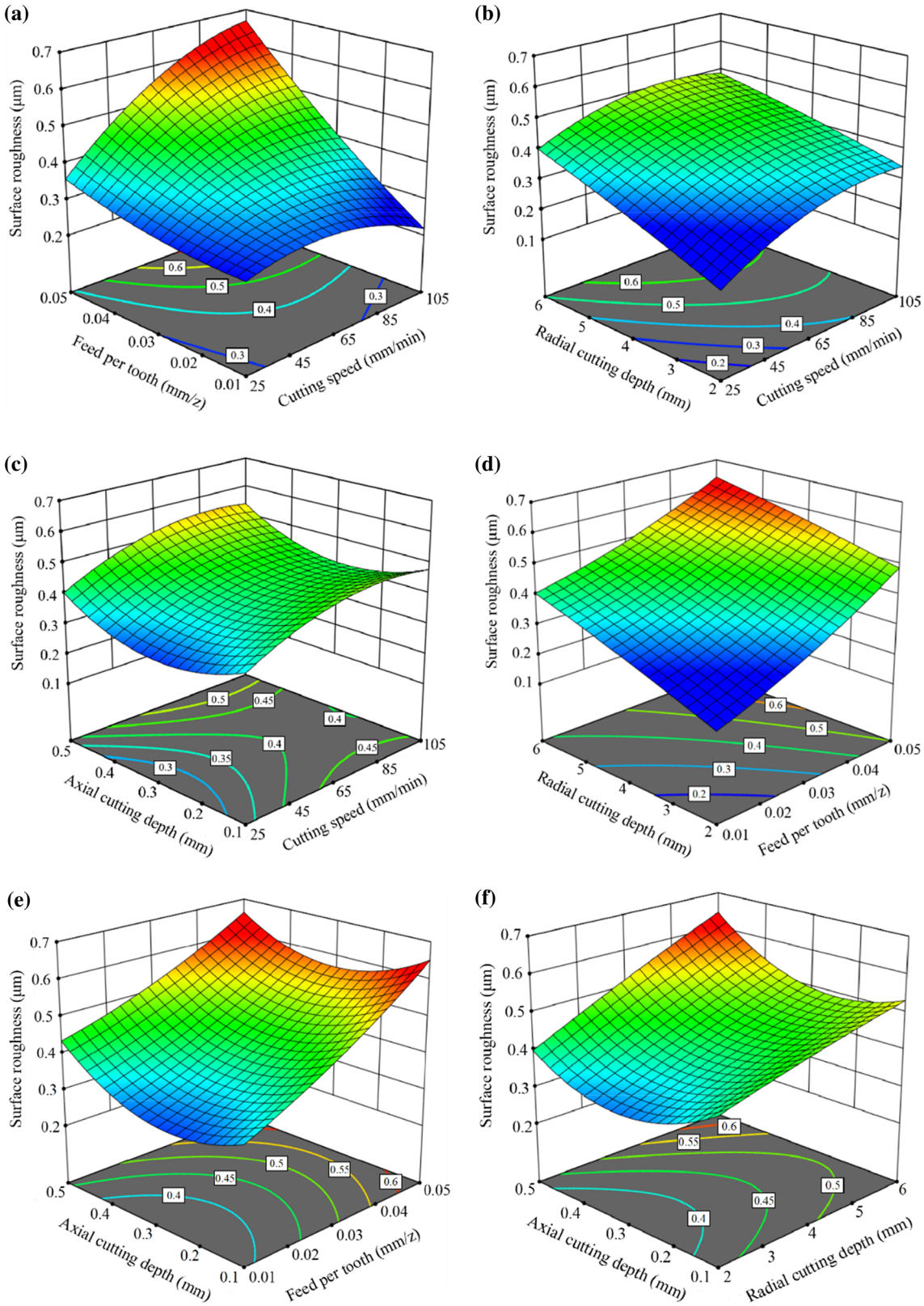

Fig. 6 Surface plots and contour plots for surface roughness against **a** speed and feed, **b** speed and radial cutting depth, **c** speed and axial cutting depth, **d** feed and radial cutting depth, **e** feed and axial cutting depth, **f** radial cutting depth and axial cutting depth

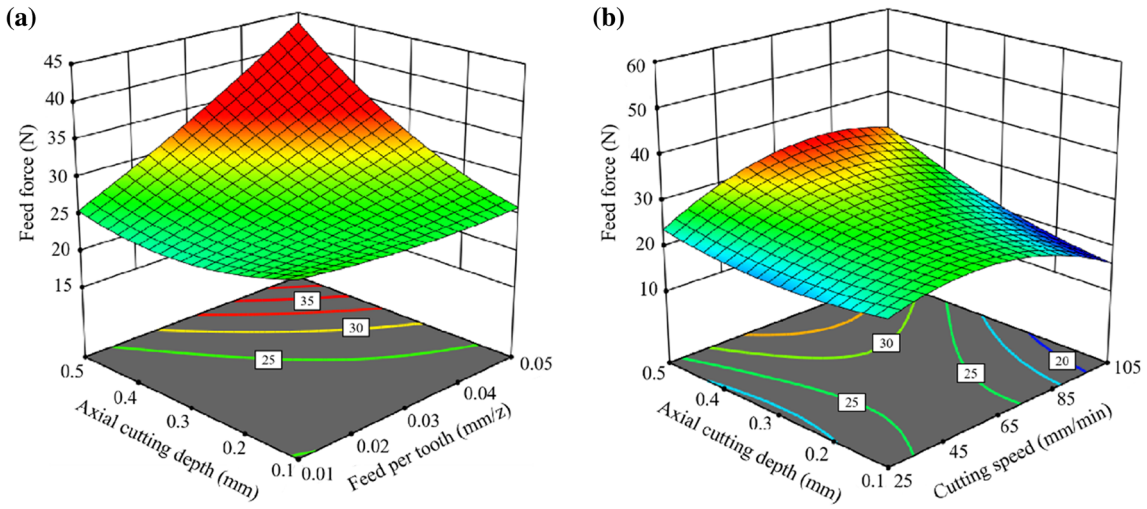

Fig. 7 Surface plots and contour plots for feed force against **a** feed and axial cutting depth, **b** speed and axial cutting depth

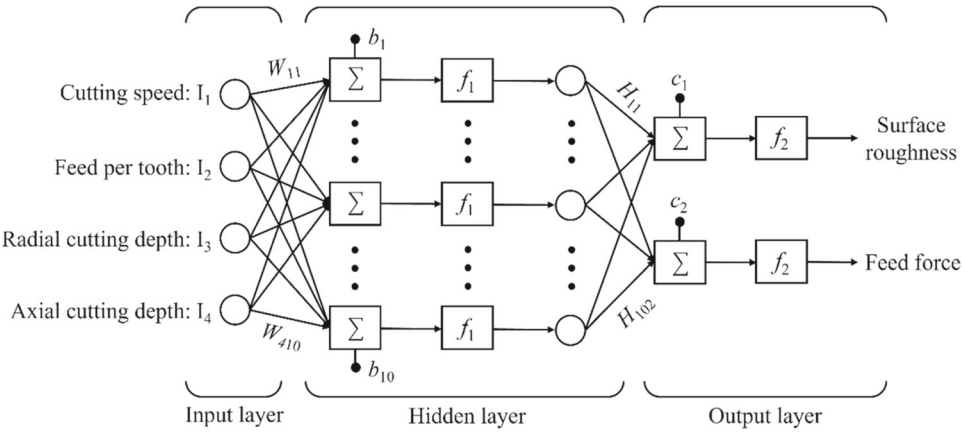

Fig. 8 BP neural network architecture

W_{ij} and b_i are weights and bias of input layer to hidden layer, respectively
H_{ij} and c_i are weights and bias of hidden layer to output layer, respectively

respectively, indicating that the ANN models have great fitting ability.

4.1 Comparison of ANN and RSM Predictive Model

The first 10 groups of experimental data are selected as the prediction accuracy (PA) verification samples of ANN and RSM models. The comparison of prediction performance in RSM and ANN models is illustrated in Table 6. Equation 9 is used to calculate the prediction accuracy ε of each dataset.

$$\varepsilon = 1 - \delta = 1 - \frac{\left|\text{Expt. value}_i - \text{Model pred}_i\right|}{\text{Expt. value}_i} \times 100\% \tag{9}$$

where δ represents the relative error between predictive and measured values.

The average accuracy μ can be obtained by the following formula:

$$\mu = \frac{1}{h}\sum_{i=1}^{h}(\varepsilon_i) \times 100\% \tag{10}$$

where h is the number of datasets contained in model.

Based on Table 6, the sample PA of RSM and ANN models is 94.58% and 97.66% for R_a, 97.17% and 99.51% for F_t. The comparison of 31 groups of experimental data and predicted data in RSM, ANN models is given in Fig. 9. For the R_a response, the PA of RSM reaches 94.43% with a maximum of 99.78%; the PA of ANN reaches 95.83% with a maximum of 100%. For the F_t response, the PA of RSM is found to be 96.68% with a maximum of 99.81%; the PA of ANN is found to be 98.06% with a maximum of 100%. It can be concluded by comparison that the developed RSM and ANN models both have good prediction ability, while the ANN predictive

Table 6 Comparison of prediction performance in RSM and ANN models

Run	Surface roughness, R_a					Feed force, F_t				
	Expt. (μm)	RSM		ANN		Expt. (*N*)	RSM		ANN	
		Pred. (μm)	Pred. acc. (%)	Pred. (μm)	Pred. acc. (%)		Pred. (*N*)	Pred. acc. (%)	Pred. (*N*)	Pred. acc. (%)
1	0.318	0.292	91.73	0.353	88.96	25.81	24.90	96.48	25.80	99.96
2	0.341	0.316	92.87	0.341	100	23.12	23.87	96.74	23.14	99.91
3	0.362	0.395	90.81	0.362	100	26.32	26.61	98.89	26.32	100
4	0.540	0.513	95.00	0.540	100	24.17	23.86	98.70	23.12	95.66
5	0.396	0.385	97.30	0.396	100	26.87	24.71	91.94	26.88	99.96
6	0.401	0.391	97.51	0.401	100	23.64	23.69	99.81	23.64	100
7	0.501	0.473	94.35	0.501	100	28.16	28.02	99.52	28.18	99.93
8	0.550	0.571	96.16	0.618	87.66	24.06	25.28	94.94	24.11	99.79
9	0.301	0.308	97.64	0.301	100	26.63	25.25	94.83	26.67	99.85
10	0.314	0.338	92.39	0.314	100	28.12	28.18	99.80	28.12	100
Sample accuracy			94.58		97.66			97.17		99.51

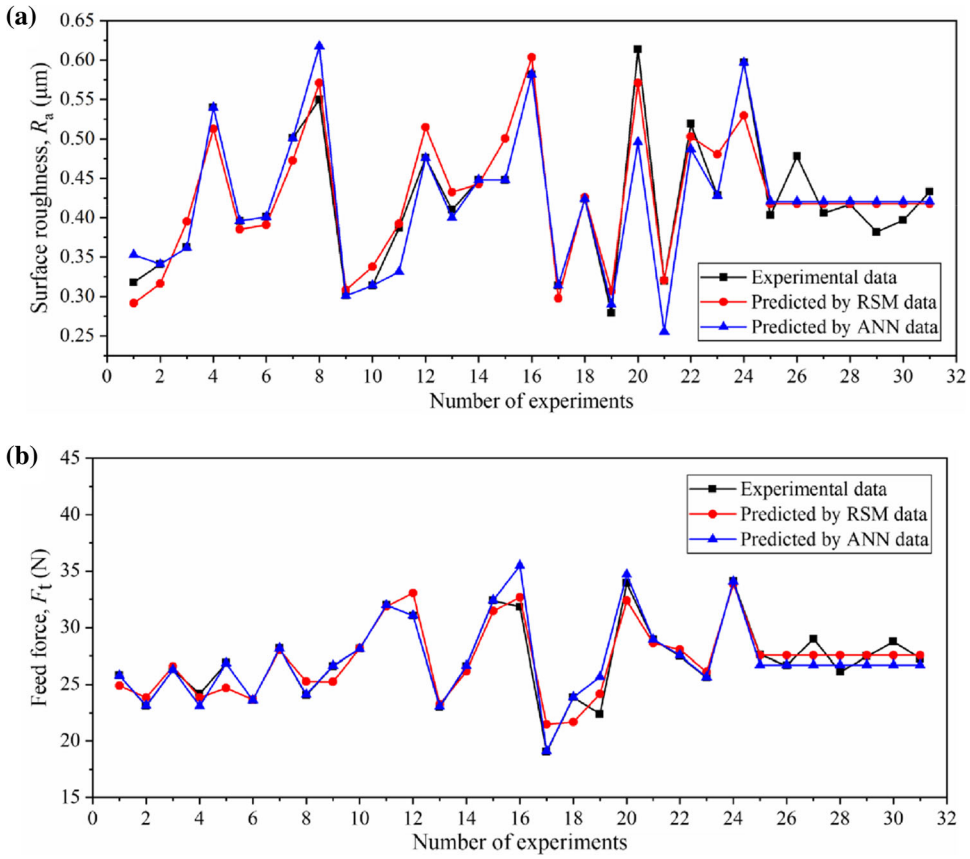

Fig. 9 Comparison between experimental, RSM and ANN data for **a** surface roughness, **b** feed force

model is more accurate than RSM model in predicting R_a and F_t.

In practical applications, the advantages of RSM and ANN can be combined to obtain more accurate and reliable results.

5 Optimization of Milling Parameters by Genetic Algorithm

Genetic algorithm (GA) is a search algorithm formed by simulating the genetic and evolutionary principles of organisms in nature [39]. GA is composed of three modules: encoding and decoding, individual fitness evaluation and genetic operation. Among them, the genetic operation includes chromosome replication, crossover and variation. The flowchart of GA operation is given in Fig. 10. In this part, Al-50wt% Si alloy milling parameters optimization for single and multiple objectives is implemented, using the global optimization method: GA.

5.1 Single-Objective Optimization With GA

The quadratic regression mathematical models of surface roughness and feed force in Eqs. 6 and 7 are taken as the objective/fitness functions. The single-objective optimization theoretical formula of R_a and F_t are described below:

$$\begin{aligned}\text{Minimize} R_a &= f_1(v_c, f_z, a_e, a_p)\\ &= \text{Min}(0.142149 + 0.00346v_c - 1.00022f_z\\ &\quad + 0.06245a_e - 1.38336a_p - 0.000035v_c^2\\ &\quad + 52.4256f_z^2 - 0.001507a_e^2\\ &\quad + 2.17426a_p^2 + 0.115938v_c f_z\\ &\quad - 0.000241v_c a_e + 0.000594v_c a_p - 0.40625f_z a_e\\ &\quad - 4.8125f_z a_p + 0.076875a_e a_p) \end{aligned} \tag{11}$$

$$\begin{aligned}\text{Minimize } F_t &= f_2(v_c, f_z, a_e, a_p)\\ &= \text{Min}(26.37705 + 0.403558v_c\\ &\quad - 292.97991f_z - 1.55645a_e - 67.89799a_p\\ &\quad - 0.003732v_c^2 + 1833.77976f_z^2\\ &\quad + 0.194628a_e^2 + 60.8378a_p^2\\ &\quad - 2.15937v_c f_z + 0.000094v_c a_e + 0.494063v_c a_p\\ &\quad + 40.1875f_z a_e + 1225.625f_z a_p\\ &\quad - 4.53125a_e a_p) \end{aligned} \tag{12}$$

The constraints of milling parameters in GA optimization process are: 25 m/min $\leq$ $v_c \leq$ 105 m/min, 0.01 mm/z $\leq f_z \leq$ 0.05 mm/z, 2 mm $\leq a_e \leq$ 6 mm, 0.1 mm $\leq a_p \leq$ 0.5 mm. The population size, crossover rate, mutation rate, iteration times and so on are the critical parameters in GA, which are shown in Table 7.

The optimization process of GA is carried out in MATLAB. For surface roughness, the optimal milling parameters obtained by GA performing 10 times are listed in Table 8. Due to the randomness of the initial production function, the R_a prediction results after each optimization are different. Fortunately, the overall difference is small with the maximum difference of 0.043 μm. Therefore, using GA to optimize Al-50wt% Si alloy milling parameters can fully meet the requirement of R_a less than 0.4 μm in this paper.

As seen in Table 8, the R_a obtained in the fourth GA run is the smallest, which reaches 0.128 μm. The corresponding v_c is 104.781 m/min, f_z is 0.01 mm/z, a_e is 2 mm, and a_p is 0.271 mm. The fitness change in the fourth GA optimization process is shown in Fig. 11. It can be seen that when the number of iterations reaches 132 generations, the optimal and average fitness values are stable, indicating that the initial parameter setting is appropriate.

It can also be found from Table 8 that when the v_c is the lowest (25 m/min) or the highest (105 m/min), and the a_p is about 0.3 mm, R_a is easy to reach the lowest value. When the f_z and a_e are the lowest, the R_a is the smallest. This is consistent with the response surface analysis in the above section.

For the single-objective optimization of feed force using GA, the process is consistent with the R_a optimization mentioned above. The minimum F_t value achieved by GA is 13.137 N. The corresponding v_c is 105 m/min, f_z is 0.05 mm/z, a_e is 2 mm, and a_p is 0.1 mm.

5.2 Multi-Objective Optimization With GA

The unified objective method can be used to solve multi-objective optimization problems. The operation principle of this method is to integrate each single objective function into a total objective function $F(x)$, as depicted in Eq. 13. Considering the different importance of each sub-objective function value, it is necessary to allocate their weights.

$$F(x) = \sum_{i=1}^{n} w_i \cdot f_i(x) \tag{13}$$

where w_i is the weighting factor of each sub-goal, and $f_i(x)$ is the sub-objective function.

In order to obtain the weight of each sub-goal, performance indicators should first be standardized (i.e., data normalization). Different evaluation indexes often have different dimensions and dimensional units, which will affect the data analysis results. Therefore, during data pre-processing, the original data must be normalized and converted into values within the range of [0,1]. Since lower R_a and F_t are desired

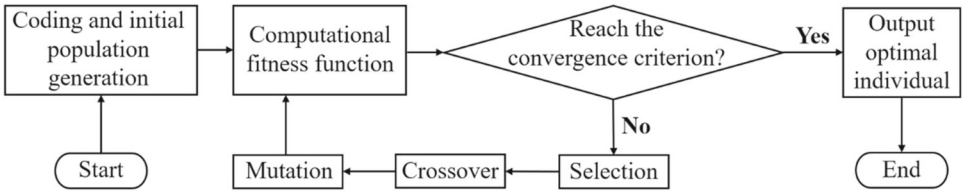

Fig. 10 Flowchart of GA operation

Table 7 Genetic algorithm parameters

GA parameter	Population size	Selection function	Elite count	Crossover fraction	Mutation fraction	Maximum genetic iterations
Description	40	Roulette	2	70%	2%	200

Table 8 Milling parameters optimized for minimizing surface roughness

Run times of GA	Cutting speed	Feed per tooth	Radial cutting depth	Axial cutting depth	Iteration times	Minimum value
1	25	0.01	2.006	0.302	84	0.147
2	29.143	0.014	2.144	0.291	146	0.171
3	25.051	0.011	2.111	0.293	64	0.155
4	104.781	0.01	2	0.271	132	0.128
5	25.2	0.013	2.019	0.296	119	0.150
6	25.122	0.011	2.129	0.291	190	0.156
7	100.987	0.01	2	0.276	168	0.139
8	104.873	0.011	2.106	0.278	176	0.146
9	103.088	0.01	2	0.28	106	0.133
10	102.5	0.01	2.19	0.276	59	0.145

during Al-50wt% alloy milling, Eq. 14 is used for data standardization [40]:

$$y_i = \frac{\max(x - x_i)}{\max(x) - \min(x)} \tag{14}$$

where x_i denotes the original data sequence and y_i is the dimensionless standardized value.

After this, entropy weight method (EWM) is applied for weight distribution. EWM can reduce the influence of subjective will and improve the objectivity of index weight distribution [41]. The original evaluation matrix $R = (r_{ij})_{m\times n}$ has m items to be evaluated and n evaluation indicators. The entropy value H_i of index i is defined in Eqs. 15 and 16. The

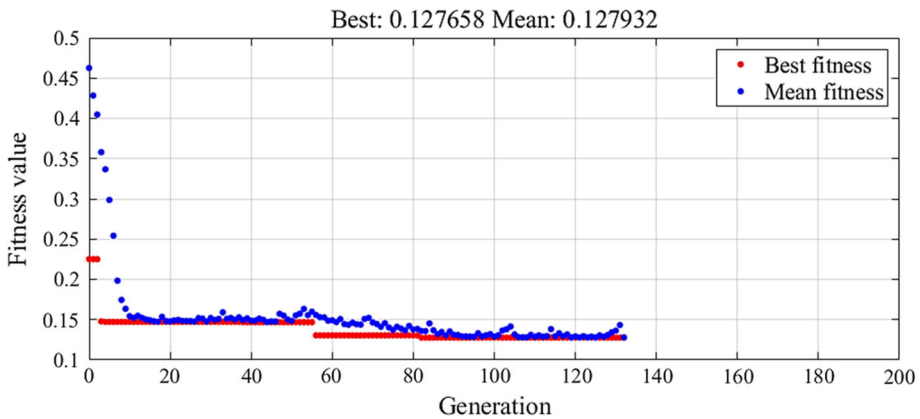

Fig. 11 Fitness change in the fourth GA optimization process

Table 9 Comparison of various optimization techniques

Method	Optimization method	Optimal parameter combination	Iteration times	Optimal responses
Single-objective optimization	GA	Minimizing R_a: v_c (104.781 m/min), f_z (0.01 mm/z), a_e (2 mm), a_p (0.271 mm)	132	$R_a = 0.127$ μm
		Minimizing F_t: v_c (105 m/min), f_z (0.05 mm/z), a_e (2 mm), a_p (0.1 mm)	151	$F_t = 13.137$ N
Multi-objective optimization	GA with EWM	Minimizing R_a and F_t: v_c (105 m/min), f_z (0.013 mm/z), a_e (3.909 mm), a_p (0.14 mm)	90	$R_a = 0.266$ μm $F_t = 18.84$ N

entropy weight w_i is presented in Eq. 17.

$$p_{ij} = \frac{r_{ij}}{\sum_{i=1}^{m} r_{ij}} \tag{15}$$

$$H_i = -\frac{1}{\ln m} \sum_{i=1}^{m} p_{ij} \cdot \ln p_{ij} \tag{16}$$

$$w_i = \frac{1 - H_i}{\sum(1 - H_i)} \tag{17}$$

The weight of surface roughness and feed force $W = [0.4995,\ 0.5005]$ is obtained. Therefore, the transformed multi-objective optimization equation can be expressed as:

$$\begin{aligned} &\text{Minimize} F(x) = 0.4995 f_1(x) + 0.5005 f_2(x) \\ &x = \left[v_c,\ f_z,\ a_e,\ a_p\right] \end{aligned} \tag{18}$$

Through GA, the optimal combination of milling parameters is $v_c = 105$ m/min, $f_z = 0.013$ mm/z, $a_e = 3.909$ mm, $a_p = 0.14$ mm. As shown in Table 9, the surface roughness and feed force predicted by GA under optimal parameters is 0.266 μm and 18.84 N, respectively. The verification milling experiment shows that the R_a is 0.275 μm and F_t is 19.76 N. Namely, the prediction errors of R_a and F_t are 3.27% and 4.65%, respectively. This shows that although there is slight noise and vibration in the multi-response optimization process, the prediction is acceptable. It can be concluded that in order to obtain the minimum R_a and F_t simultaneously, the set of parameters can be used as the optimal value for precision milling Al-50wt% Si alloy.

6 Conclusion

This paper aims to optimize the precision milling parameters of high Si-Al alloy. RSM and ANOVA were used to study the influence of four cutting parameters on surface roughness R_a and feed force F_t in milling Al-50wt% Si alloy. Then, the predictive modeling was developed and compared utilizing RSM and ANN. Employing GA and EWM techniques, the single-objective and multi-objective parameter optimizations were carried out. Through experiments, the accuracy of the prediction model and method can be verified. The conclusions are as follows:

(1) Among different RSM models, the quadratic models are found better in fitting degree and predicting performance. Feed per tooth provides a primary contribution to R_a. Axial cutting depth has the most significant effect on F_t.
(2) When f_z is small, v_c is the lowest (25 m/min) or highest (105 m/min), the minimum R_a will be produced. However, simultaneously increasing f_z and v_c will worsen the R_a.
(3) In the response value of F_t, $f_z a_p$ and $v_c a_p$ are significant interaction items. Increasing both f_z and a_p can increase the F_t. Lower or higher v_c combined with lower a_p results in lower F_t.
(4) ANN predictive model is more accurate than RSM model for milling Al-50wt% Si alloy. The ANN average prediction accuracy for R_a and F_t reaches 95.83% and 98.06%, respectively.
(5) Single-objective parameter optimization using GA obtains minimum R_a and F_t as 0.127 μm and 13.137 N, respectively.
(6) Based on GA and EWM in multi-objective optimization, the optimal parameter combination as $v_c = 105$ m/min, $f_z = 0.013$ mm/z, $a_e = 3.909$ mm, $a_p = 0.14$ mm is obtained. The response values under this set of parameters for R_a and F_t are 0.275 μm and 19.76 N. Confirmation test shows the prediction error of R_a and F_t is 3.27% and 4.65%, respectively, which illustrates the method has great effectiveness.

The above research conclusions will provide theoretical and technical support for improving the surface quality and cutting parameters of precision milling Al-50wt% Si alloy.

Author Contributions LJ was involved in conceptualization, methodology, investigation, data curation, writing—original draft. QN helped

in conceptualization, methodology, supervision, funding acquisition, writing—review and editing. DZ contributed to investigation, methodology. SL was involved in validation, writing—review and editing. WY helped in supervision.

Funding This work was supported by the National Natural Science Foundation of China (No. 52075168, 51605161), the Project of Department of Education of Hunan Province (No. 19B190), and the Scientific Research Fund of Hunan University of Science and Technology (No. KJ-2042).

Availability of data and material The data and material in this paper are original, available and objective.

Code availability Not applicable.

Declarations

Conflict of interests The authors have no relevant financial or non-financial interests to disclose.

Ethical Approval Not applicable.

Consent to Participate Not applicable.

Consent for Publication We would like to submit the manuscript entitled 'Predictive modeling of surface roughness and feed force in Al-50wt% Si alloy milling based on response surface method and various optimal algorithms' by Lu Jing, Qiulin Niu, Dilei Zhan, Shujian Li, Wenhui Yue, and we wish to be considered for publication in the 'Arabian Journal for Science and Engineering.'

References

1. Sun, W.; Duan, C.Z.; Yin, W.D.: Chip formation mechanism in machining of Al/SiC_p composites based on analysis of particle damage. J. Manuf. Process. **64**, 861–877 (2021). https://doi.org/10.1016/j.jmapro.2021.02.032
2. Niu, Q.; Jing, L.; Li, C.; Yu, Z.; Yue, W.: Study on effects of tool nose radius on the formation mechanism of edge defects during milling SiC_p/Al composites. Int. J. Adv. Manuf. Tech. **114**, 2261–2269 (2021). https://doi.org/10.1007/s00170-021-07018-1
3. Fan, Y.; Xu, Y.; Hao, Z.; Lin, J.: Cutting deformation mechanism of SiC_p/Al composites based on strain gradient theory. J. Mater. Process. Tech. **299**, 117345 (2021). https://doi.org/10.1016/j.jmatprotec.2021.117345
4. Yu, K.; Li, C.; Wang, R.; Yang, J.: Production and properties of a spray formed 70% Si-Al alloy for electronic packaging applications. Mater. Trans. **49**, 685–687 (2008). https://doi.org/10.2320/matertrans.MRP2007630
5. Jcw, A.; Sc, A.; Tjk, A.; Ms, B.; Atc, B.: Influence of contact area on the sliding friction and wear behaviour of an electrochemical jet textured Al-Si alloy. Wear **426–427**, 1336–1344 (2019). https://doi.org/10.1016/j.wear.2019.01.008
6. Muratoğlu, M.; Yilmaz, O.; Aksoy, M.: Investigation on diffusion bonding characteristics of aluminum metal matrix composites (Al/SiC_p) with pure aluminum for different heat treatments. J. Mater. Process. Tech. **178**, 211–217 (2006). https://doi.org/10.1016/j.jmatprotec.2006.03.168
7. Kulisz, M.; Zagórski, I.; Korpysa, J.: The effect of abrasive waterjet machining parameters on the condition of Al-Si alloy. Materials **13**, 3122 (2020). https://doi.org/10.3390/ma13143122
8. Zhou, Y.; Sun, H.; Li, A.; Lv, M.; Zhao, J.: FEM simulation-based cutting parameters optimization in machining aluminum-silicon piston alloy ZL109 with PCD tool. J. Mech. Sci. Technol. **33**, 3457–3465 (2019). https://doi.org/10.1007/s12206-019-0640-3
9. Niu, Z.; Cheng, K.: Improved dynamic cutting force modelling in micro milling of metal matrix composites Part I: Theoretical model and simulations. P. I. Mech. Eng. C-J. Mec. **234**, 1733–1745 (2020). https://doi.org/10.1177/0954406219899688
10. Ononiwu, N.H.; Ozoegwu, C.G.; Madushele, N.; Akinlabi, E.T.: Characterization, machinability studies, and multi-response optimization of AA 6082 hybrid metal matrix composite. Int. J. Adv. Manuf. Tech., 1–19 (2021). https://doi.org/10.1007/s00170-021-07549-7
11. Naresh, N.; Jenarthanan, M.P.; Prakash, R.H.: Multi-objective optimisation of CNC milling process using Grey-Taguchi method in machining of GFRP composites. Multidiscip. Model. Mater. Struct. **10**, 265–275 (2014). https://doi.org/10.1108/MMMS-06-2013-0042
12. Kumar, S.L.: Measurement and uncertainty analysis of surface roughness and material removal rate in micro turning operation and process parameters optimization. Measurement **140**, 538–547 (2019). https://doi.org/10.1016/j.measurement.2019.04.029
13. Uzun, M.; Usca, S.A.; Kuntolu, M.; Gupta, M.K.: Influence of tool path strategies on machining time, tool wear, and surface roughness during milling of AISI X210Cr12 steel. Int. J. Adv. Manuf. Tech. **119**, 2709–2720 (2022). https://doi.org/10.1007/s00170-021-08365-9
14. Dang, J.; Zhang, H.; An, Q.; Ming, W.; Chen, M.: On the microstructural evolution pattern of 300M steel subjected to surface cryogenic grinding treatment. J. Manuf. Process. **68**, 169–185 (2021). https://doi.org/10.1016/j.jmapro.2021.05.026
15. Singh, D.; Chadha, V.; Msingari, R.: Effect of nose radius on surface roughness during CNC turning using response surface methodology. Int. J. Recent Adv. Mech. Eng. **5**, 31–45 (2016). https://doi.org/10.14810/ijmech.2016.5203
16. Kumar, R.; Chauhan, S.: Study on surface roughness measurement for turning of Al 7075/10/SiC_p and Al 7075 hybrid composites by using response surface methodology (RSM) and artificial neural networking (ANN). Measurement **65**, 166–180 (2015). https://doi.org/10.1016/j.measurement.2015.01.003
17. Chandrasekaran, M.; Devarasiddappa, D.: Development of predictive model for surface roughness in end milling of Al-SiC_p metal matrix composites using fuzzy logic. World Acad. Sci. Eng. Technol. **6**, 928–933 (2012). https://www.researchgate.net/publication/265603018
18. Rajmohan, T.; Palanikumar, K.: Modeling and analysis of performances in drilling hybrid metal matrix composites using D-optimal design. Int. J. Adv. Manuf. Tech. **64**, 1249–1261 (2013). https://doi.org/10.1007/s00170-012-4083-6
19. Pare, V.; Agnihotri, G.; Krishna, C.: Selection of optimum process parameters in high speed CNC end-milling of composite materials using meta heuristic techniques-A comparative study. Strojniški vestnik. J. Mech. Eng. **61**, 176–186 (2015). https://doi.org/10.5545/sv-jme.2014.1914
20. Zhu, C.; Gu, P.; Wu, Y.; Liu, D.; Wang, X.: Surface roughness prediction model of SiC_p/Al composite in grinding. Int. J. Mech. Sci. **155**, 98–109 (2019). https://doi.org/10.1016/j.ijmecsci.2019.02.025
21. Mia, M.; Gupta, M.K.; Lozano, J.A.; Carou, D.; Pimenov, D.Y.; Królczyk, G.; Khan, A.M.; Dhar, N.R.: Multi-objective optimization and life cycle assessment of eco-friendly cryogenic N_2 assisted turning of Ti-6Al-4V. J. Clean. Prod. (2018). https://doi.org/10.1016/j.jclepro.2018.10.334
22. Bhattacharya, S.; Das, P.P.; Chatterjee, P.; Chakraborty, S.: Prediction of responses in a sustainable dry turning operation: A

comparative analysis. Math. Probl. Eng. 9967970 (2021). https://doi.org/10.1155/2021/9967970
23. Das, P.P.; Das, S.; Mahto, P.K.; Kumar, D.; Roy, M.K.: ANFIS-based models for coating quality prediction for thin-film deposition processes. J. Multiscale. Model. **12**, 2150007 (2021). https://doi.org/10.1142/S1756973721500074
24. Tamang, S.K.; Chandrasekaran, M.: Modeling and optimization of parameters for minimizing surface roughness and tool wear in turning Al/SiC_p MMC, using conventional and soft computing techniques. Adv. Prod. Eng. Manag. **10**, 59–72 (2015). https://doi.org/10.14743/apem2015.2.192
25. Muguthu, J.N.; Dong, G.; Ikua, B.: Optimization of machining parameters influencing machinability of Al2124SiC_p (45%wt) metal matrix composite. J. Compos. Mater. **49**, 217–229 (2015). https://doi.org/10.1177/0021998313516141
26. Dang, J.; Zang, H.; An, Q.; Ming, W.; Chen, M.: Feasibility study of creep feed grinding of 300M steel with zirconium corundum wheel. Chin. J. Aeronaut. **35**, 565–578 (2022).https://doi.org/10.1016/j.cja.2021.01.029
27. Dang, J.; Zhang, H.; An, Q.; Ming, W.; Chen, M.: Surface modification of ultrahigh strength 300M steel under supercritical carbon dioxide ($scCO_2$)-assisted grinding process. J. Manuf. Process. **61**, 1–14 (2021). https://doi.org/10.1016/j.jmapro.2020.11.001
28. Daniel, S.A.A.; Pugazhenthi, R.; Kumar, R.; Vijayananth, S.: Multi-objective prediction and optimization of control parameters in the milling of aluminium hybrid metal matrix composites using ANN and Taguchi-grey relational analysis. Def. Technol. **15**, 545–556 (2019). https://doi.org/10.1016/j.dt.2019.01.001
29. Karabulut, Sener.: Optimization of surface roughness and cutting force during AA7039/Al_2O_3 metal matrix composites milling using neural networks and taguchi method. Measurement **66**, 139–149 (2015). https://doi.org/10.1016/j.measurement.2015.01.027
30. Tsao, C.C.; Hocheng, H.: Evaluation of thrust force and surface roughness in drilling composite material using Taguchi analysis and neural network. J. Mater. Process. Tech. **203**, 342–348 (2008). https://doi.org/10.1016/j.jmatprotec.2006.04.126
31. Premnath, A.A.; Alwarsamy, T.; Rajmohan, T.: Experimental investigation and optimization of process parameters in milling of hybrid metal matrix composites. Mater. Manuf. Process. **27**, 1035–1044 (2012). https://doi.org/10.1080/10426914.2012.677911
32. Jia, Y.; Cao, F.; Scudino, S.; Ma, P.; Li, H.; Yu, L.; Eckert, J.; Sun, J.: Microstructure and thermal expansion behavior of spray-deposited Al-50Si. Mater. Des. **57**, 585–591 (2014). https://doi.org/10.1016/j.matdes.2013.12.066
33. Xu, Z.; Wang, Z.: Experimental study on high speed milling of aluminum silicon alloy for T/R Modules. Electro-Mech. Eng. **34**, 43–46 (2018). https://doi.org/10.19659/j.issn.1008-5300.2018.06.011
34. Liu, C.; Gao, L.; Jiang, X.; Xu, W.; Yang, T.: Analytical modeling of subsurface damage depth in machining of SiC_p/Al composites. Int. J. Mech. Sci. **185**, 105874 (2020). https://doi.org/10.1016/j.ijmecsci.2020.105874
35. Ghufran, M.; Uddin, G.M.: Comparative performance analysis of cemented carbide, TiN, TiAlN, and PCD coated inserts in dry machining of Al 2024 alloy. Int. J. Adv. Manuf. Tech. (2021). https://doi.org/10.1007/s00170-020-06315-5
36. Wang, J.; Shang, Z.; Lv, P.; Fan, X.: Analysis and experimental research on affection on approach angle of tool nose radius. J. Graph. **40**, 256–260 (2019). https://doi.org/10.11996/JG.j.2095-302X.2019020256
37. Gopan, V.; Wins K, L.; Evangeline, G.; Surendran, A.: Experimental investigation for the multi-objective optimization of machining parameters on AISI D2 steel using particle swarm optimization coupled with artificial neural network. J. Adv. Manuf. Syst. **19**, 589–606 (2020). https://doi.org/10.1142/S0219686720500286
38. Barma, S.D.; Das, B.; Giri, A.; Majumder, S.; Bose, P.K.: Back propagation artificial neural network (BPANN) based performance analysis of diesel engine using biodiesel. J. Renew. Sustain. Ener. **3**, 1–12 (2011). https://doi.org/10.1063/1.3517229
39. Palanisamy, P.; Rajendran, I.; Shanmugasundaram, S.: Optimization of machining parameters using genetic algorithm and experimental validation for end-milling operations. Int. J. Adv. Manuf. Tech. **32**, 644–655 (2007). https://doi.org/10.1007/s00170-005-0384-3
40. Ren, J.; Zhou, J.; Zeng, J.: Analysis and optimization of cutter geometric parameters for surface integrity in milling titanium alloy using a modified grey-Taguchi method. P. I. Mech. Eng. B-J. Eng. **230**, 2114–2128 (2016). https://doi.org/10.1177/0954405415599927
41. Suneesh, E.; Sivapragash, M.: Multi-response optimisation of micro-milling performance while machining a novel magnesium alloy and its alumina composites. Measurement **168**, 108345 (2020). https://doi.org/10.1016/j.measurement.2020.108345